

A Generalized SiGe HBT Single-Event Effects Model for On-Orbit Event Rate Calculations

Jonathan A. Pellish, *Student Member, IEEE*, Robert A. Reed, *Senior Member, IEEE*, Akil K. Sutton, *Student Member, IEEE*, Robert A. Weller, *Senior Member, IEEE*, Martin A. Carts, *Member, IEEE*, Paul W. Marshall, *Member, IEEE*, Cheryl J. Marshall, Ramkumar Krithivasan, *Student Member, IEEE*, John D. Cressler, *Fellow, IEEE*, Marcus H. Mendenhall, Ronald D. Schrimpf, *Fellow, IEEE*, Kevin M. Warren, *Member, IEEE*, Brian D. Sierawski, *Member, IEEE*, and Guofu F. Niu, *Senior Member, IEEE*

Abstract—This work draws on experimental and simulation results to derive a generalized SEU response model for bulk SiGe HBTs. The model was validated using published heavy ion and new proton data gathered from high-speed HBT digital logic integrated circuits fabricated in the IBM 5AM SiGe BiCMOS process. Calibrating to heavy ion data was sufficient to reproduce the proton data without further adjustment. The validated model is used to calculate upset event rates for low-earth and geosynchronous orbits under typical conditions.

Index Terms—Deep trench isolation, Geant4, geosynchronous orbit, low-earth orbit, rate prediction, silicon-germanium HBT, single-event upset.

I. INTRODUCTION

A. Overview

SILICON-GERMANIUM heterojunction bipolar transistor (SiGe HBT) technology, due to its inherent total ionizing dose (TID) tolerance [1]–[3], high-speed capability [4]–[8], superior low-temperature performance [6], [10], and seamless integration with deep sub-micrometer CMOS makes it a suitable candidate for space-based applications.

However, despite these appealing characteristics, heavy ion tests on GHz-speed current mode logic (CML) master–slave D flip-flop (DFF) shift registers, fabricated in several generations of SiGe HBTs, showed single-event upset (SEU) thresholds below linear energy transfers (LET) of $2 \text{ MeV} \cdot \text{cm}^2/\text{mg}$

Manuscript received July 20, 2007; revised September 13, 2007 and October 4, 2007. This work was supported in part by the NASA Electronic Parts and Packaging Program and the Defense Threat Reduction Agency Radiation Hardened Microelectronics Program under IACRO #07-4201i to NASA, as well as the Georgia Electronic Design Center at the Georgia Institute of Technology.

J. A. Pellish, R. A. Reed, R. A. Weller, and R. D. Schrimpf are with the Department of Electrical Engineering and Computer Science, Vanderbilt University, Nashville, TN 37235 USA (e-mail: jonathan.pellish@ieee.org).

A. K. Sutton, R. Krithivasan, and J. D. Cressler are with the School of Electrical and Computer Engineering, Georgia Institute of Technology, Atlanta, GA 30332 USA.

M. A. Carts and C. J. Marshall are with the NASA Goddard Space Flight Center, Greenbelt, MD 20771 USA.

P. W. Marshall is a NASA consultant in Brookneal, VA 24528 USA.

M. H. Mendenhall, K. M. Warren, and B. D. Sierawski are with the Institute for Space and Defense Electronics, Vanderbilt University, Nashville, TN 37235 USA.

G. F. Niu is with the Electrical and Computer Engineering Department, Auburn University, Auburn, AL 36849 USA.

Color versions of one or more of the figures in this paper are available online at <http://ieeexplore.ieee.org>.

Digital Object Identifier 10.1109/TNS.2007.909987

and saturated cross sections above $200 \mu\text{m}^2$ for single shift register stages [4]–[9]. Significant SEU susceptibility has always been an issue when considering SiGe HBT or SiGe BiCMOS applications, but the issue can be managed if the likely SEU event rates for planned mission environments are known. This work describes the development of a generalized energy deposition SEU response model for SiGe HBTs that can be used to calculate event rates for various well-defined environments. The response model was designed for use with our simulation framework [10]–[14], which includes the Monte Carlo radiative energy deposition (MRED) tool [10]–[12], [15], [16].

The generalized model developed in this work was applied to two different DFF shift register designs fabricated in the IBM 5AM SiGe BiCMOS (IBM 5AM) process: a baseline design and a radiation hardened by design (RHBD) variant. This process is characterized by a $0.5 \mu\text{m}$ drawn emitter width, a unity-gain cutoff frequency of 50 GHz, and a BV_{CB0} of 3.3 V [1], [17].

Of the two IBM 5AM designs considered here, one was a baseline, nominal switching current, DFF shift register design [7] and the other employed a RHBD dual-interleaving technique that included duplicated pass and storage cells, which effectively decoupled the differential inputs and outputs in the storage cell [7], [18]. This input/output decoupling increased the critical charge (Q_{crit}) of this design. For the sake of simplicity, these designs are referred to as “baseline design” and “RHBD design” throughout. Both shift register designs are 127-bits long and were fabricated solely out of IBM 5AM SiGe HBTs; no complementary metal–oxide–semiconductor (CMOS) transistors were used.

B. Context and Motivation

It is important to understand the basic physical structure of a typical bulk SiGe HBT since the single-event response is driven mostly by structural processing geometry [19]. A technology computer-aided design (TCAD) cross section of the IBM 5AM process is shown in Fig. 1. Three features dominate single-event charge collection: the deep trench isolation (DTI), the lightly doped substrate, and the large area of the reverse-biased subcollector junction that is a minimum of approximately $10 \mu\text{m}^2$.

Microbeam data sets [19]–[25] of several different bulk SiGe HBT process generations have shown that individual devices exhibit significant charge collection from lateral distances on the order of $10 \mu\text{m}$ and significant vertical collection to depths of approximately $15 \mu\text{m}$ under the active region of the device.

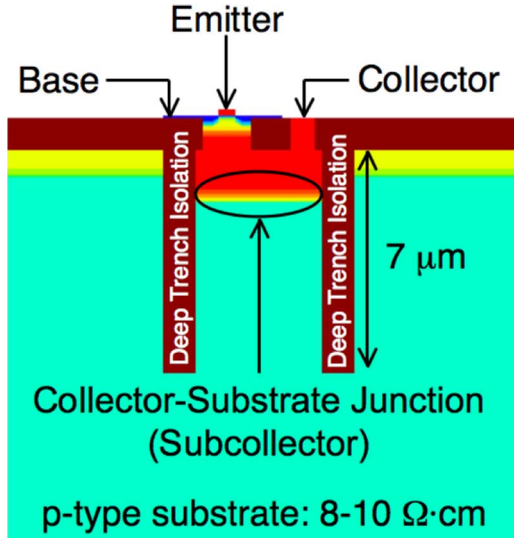


Fig. 1. TCAD cross section of the IBM 5AM SiGe HBT. Single-event charge collection is driven by the lightly doped substrate that allows for long minority carrier lifetimes and the large area of the subcollector junction. For a minimum-sized device, this junction is has an area of approximately $10 \mu\text{m}^2$.

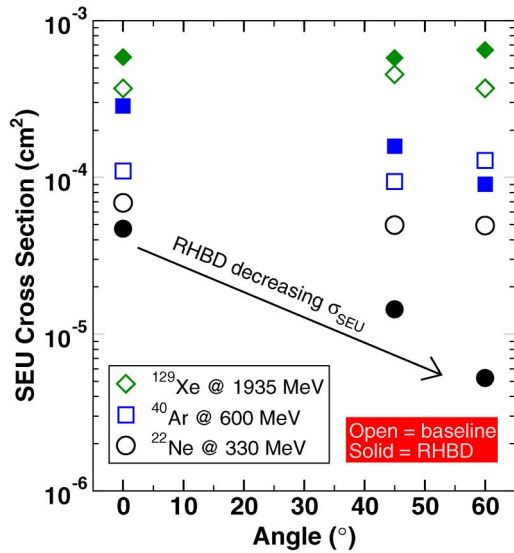


Fig. 2. Broadbeam heavy ion data for the baseline and RHBD 127-stage shift register designs after [7]. The important feature is the cross section decrease with increasing angle for the RHBD device with a higher critical charge. This roll-off behavior violates RPP model assumptions, so all RPP cosine corrections have been removed. The data are plotted with respect to angle and the cross section was scaled by $\cos(\theta)$ to remove the effective fluence correction.

These lateral and vertical charge collection distances are governed by the lightly doped substrate and the 3–5 V dropped across the subcollector space charge region (SCR). While the microbeam data sets provide unique insight into charge collection mechanisms [5], [20]–[23], [25], it is difficult to obtain reliable angular microbeam data sets, so broadbeam experiments must be used. A limited amount of small-angle microbeam data was presented in [19].

The primary broadbeam heavy ion data set [7] upon which this work is based is shown in Fig. 2. It is obvious that with the low LET neon ion the cross section of the RHBD design does not increase with increasing angle, but instead *decreases*

with *increasing* angle—i.e., decreasing cross section with increasing effective LET. This behavior violates the assumptions of the original rectangular parallelepiped (RPP) model, which generally assumes increasing cross sections with increasing effective LET [26]–[28]. This lack of agreement between the RPP model and data was discussed in detail in [19]. Since these data are not described adequately by the default RPP model, they have been re-plotted with the RPP cosine corrections removed. The data are plotted as a function of angle instead of effective LET and the cross section was scaled by $\cos(\theta)$ to remove the effective fluence correction. All subsequent data sets will be plotted in this manner to avoid confusion. For the sake of reference, the normally-incident LETs for the ions in Fig. 2 are $^{22}\text{Ne} = 2.8 \text{ MeV} \cdot \text{cm}^2/\text{mg}$, $^{40}\text{Ar} = 8.3 \text{ MeV} \cdot \text{cm}^2/\text{mg}$, and $^{129}\text{Xe} = 53 \text{ MeV} \cdot \text{cm}^2/\text{mg}$.

While the microbeam data provide adequate information to develop an energy deposition response model for normally-incident particles, most of the particles in an isotropic environment, like geosynchronous orbit, are incident at large angles. The solid angle of a cone, shown below in (1)

$$\Omega = 2\pi \left[1 - \cos\left(\frac{a}{2}\right) \right] \quad (1)$$

can be used to approximate a plane of sensitive volumes. When the apex, a , is equal to 120° , $\Omega = \pi$, which is half the solid angle subtended by the surface of a hemisphere. This means that half of the particles in an isotropic environment will be incident at angles below 60° and the other half at angles above 60° . Since a large number of particles are incident at oblique angles, understanding the angular response of bulk SiGe HBTs is critical to developing a representative rate prediction model.

It is interesting to note that some of the atypical angular response observed in Fig. 2 for the RHBD design can be accounted for by using RPP model geometry corrections proposed by Sexton [29] and Petersen [27]. The trigonometric cross section scaling factors work well for the decrease in the argon cross section, but do not account for the approximate $10\times$ decrease in the neon cross section. However, though these model extensions help to explain some of the data, they only apply to a single ion in a limited case. The model sought here must be able to handle any angle of incidence by any ion in the galactic and low-earth spectrums. The model must be unified in a way that has not been attempted before in the context of SiGe BiCMOS technologies. To understand why the traditional RPP model extensions fail to account for effects observed in these SiGe HBT data, device-level modeling is required.

II. DEVICE MODELING

A. Ion-Device Interactions

The two types of ion-device interactions considered are normally-incident and large-angle heavy ion strikes with stopping powers of $0.028 \text{ pC}/\mu\text{m}$, which is consistent with the 330 MeV ^{22}Ne used in [7], where the large cross section deviations occurred. The large angle strike is at 60° relative to the surface normal of the device in order to maintain consistency with the broadbeam data set shown in Fig. 2.

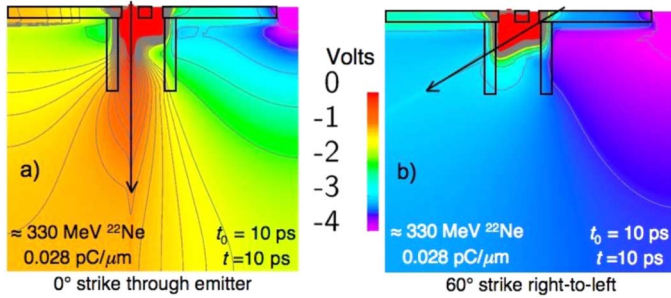


Fig. 3. These slices from 3-D TCAD simulations show the electrostatic equipotential contour lines at the peak of the temporal-Gaussian ion strike, $t = 10$ ps, which is centered at $t_0 = 10$ ps and has a width of 2 ps. In both images, (a) and (b), the substrate p-tap is located on the right side of the figure, where the potential is pinned at -4 V. The normally incident strike through the emitter produces potential warping, or push-out, into the substrate, down to a depth of approximately $18 \mu\text{m}$ in (a). In contrast, the 60° strike shown in (b) exhibits none of the potential warping seen in (a). The ion-DTI interaction essentially cuts off any subcollector junction response that could affect the electrostatic potential in the substrate.

Position-dependent, normally-incident heavy ion data for the IBM 5AM process are available through the microbeam data sets in Fig. 7 in [21], Fig. 2(c) in [20], and Fig. 3(a) in [19]. These data show that $36 \text{ MeV } ^{16}\text{O}$ strikes within the region bounded by the DTI result in a charge collection efficiency of approximately 80%, assuming that about 1 pC of charge is liberated during the stopping range of the oxygen ion, which is approximately $25 \mu\text{m}$ in pure silicon.

Normally-incident $36 \text{ MeV } ^{16}\text{O}$ strikes outside the DTI have a maximum charge collection efficiency of approximately 20%. That efficiency falls off to a few percent at $\geq 8 \mu\text{m}$ outside the DTI. Though the IBM 5AM microbeam data sets referenced in the previous paragraph only report a measurable charge collection signal up to $8 \mu\text{m}$ outside the DTI, other microbeam data sets with the same substrate resistivity and DTI geometry in [20], most notably the bulk SiGe HBTs in Fig. 2(a) and 2(b) therein, show measurable charge collection in excess of $15 \mu\text{m}$ outside the DTI.

Reliable position-dependent charge collection data gathered at a specific angle, even small angles less than 20° , are difficult to obtain with the microbeam due to spatial and mounting constraints within the beamline vacuum chamber. Therefore, angular effects need to be inferred from broadbeam data and confirmed with 3-D TCAD simulations.

The two heavy ion broadbeam conditions of interest were simulated in the IBM 5AM TCAD model described in [19]–[21] using a particle track with $dQ/dx = 0.028 \text{ pC}/\mu\text{m}$. The device was biased in the CML off-state: $V_{E,B,C} = 0 \text{ V}$ and $V_{Sx} = -4 \text{ V}$. The substrate voltage was taken from the test conditions for the DFF shift registers in [7]. The off-state was previously determined to be the most sensitive operating condition [9], [18], [22]. The simulations were carried out using the Synopsys TCAD tool suite and version X-2005.10 of Sentarus Device. The results of the simulations are shown in Fig. 3(a) and (b).

Comparing Fig. 3(a) and (b) is a straightforward, visual explanation of the cross section roll-off observed in the heavy ion broadbeam data plotted in Fig. 2. For normally-incident strikes, the potential dropped across the subcollector SCR will often

push-out into the substrate resulting in a large amount of collected charge. This push-out is very similar to the mechanism described by Hsieh [30]–[32] and Hu [33], published in the context of alpha particles. This topic, in the context of SiGe HBTs, has been discussed [19], [20]. At large angles though, the potential push-out into the substrate is mitigated by the ion passing through the DTI. In this case, since a large portion of the charge liberated by the ion appears outside of the DTI and far away from the SCR of the subcollector junction, a sufficiently large potential-compensating charge density cannot be maintained in the SCR, resulting in no potential push-out.

This same mechanism occurs in both the baseline and RHBD IBM 5AM designs; however, the difference in Q_{crit} between each design, $Q_{\text{crit}}(\text{baseline}) < Q_{\text{crit}}(\text{RHBD})$, means that each will have a different response. At normal incidence, each design behaves in the conventional manner—larger amounts of charge liberated in the substrate result in higher cross sections. However, at oblique angles, though approximately the same amount of charge is liberated, the charge collection efficiency of that charge is much lower since the device response is different, and much less dramatic.

At low dQ/dx , as in the case of $330 \text{ MeV } ^{22}\text{Ne}$, which is close to the design SEU threshold, the angular response of the RHBD design makes a large difference in the cross section trend since the amount of charge collected drops with increasing angle, approaching the value of Q_{crit} . The baseline design, though it experiences the same angular response as the RHBD design, still collects enough charge to sufficiently exceed Q_{crit} , which maintains the normal-incidence cross section.

B. Energy Deposition Response Model

This work relied on the energy transport and calorimetry capabilities of the MRED tool set, which are described in [10]–[16]. Using this tool, it is possible to compute the energy deposited in one or more sensitive (fiducial) volumes due to impinging ions. Furthermore, these fiducial volumes can have weights. The volumes and their weights function in an ensemble to form a linear combination that approximates the total collected charge. This idea was first reported in [13], and subsequently in [14]. The approach is described by (2). The total collected charge is the sum over all fiducial volumes of the product of the weight and total charge liberated.

$$Q_{\text{coll}} = \sum_i \alpha_i Q_{L_i}. \quad (2)$$

The total charge liberated (Q) is related to the total energy deposited (ED) through the relationship $Q = (1 \text{ pC}/22.5 \text{ MeV}) \times ED$. This linear combination of weighted fiducial volumes is the construct that will be used to model the energy deposition response of the SiGe HBTs considered in this work. Once calibrated to data, usually heavy ion broadbeam cross section data, this modeling method provides an accurate, high-speed approximation to the initial conditions and ensuing temporal evolution of charge transport and collection.

A 2-D projection of the basic energy deposition response model is shown in Fig. 4. The fiducial volumes have been overlaid on the TCAD cross section from Fig. 1. The top-down area

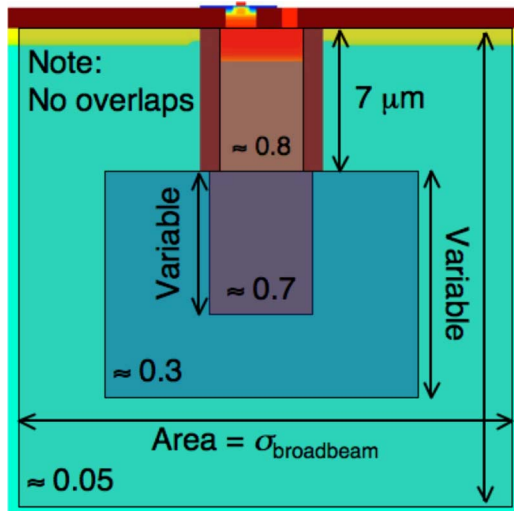


Fig. 4. This is the basic weighted fiducial volume ensemble used to model the radiation response of the IBM 5AM SiGe HBT process considered in this work. The top-down area is estimated from the normal-incidence cross section of each ion in the broadbeam heavy ion data set—three estimations in this case. The weights (efficiencies) of each of the volumes were derived from microbeam data and previous TCAD simulations [19], [20].

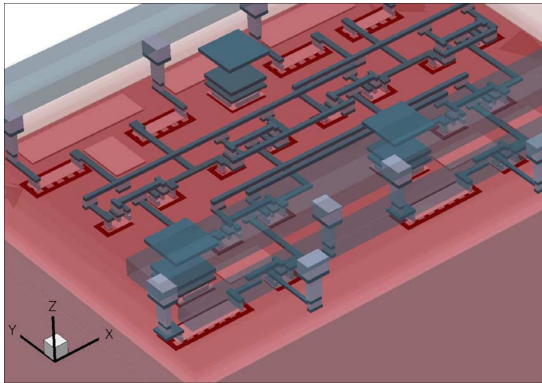


Fig. 5. Full 3-D solid geometry model of the baseline shift register design. The interlevel dielectric and metal have been made transparent. This model, and the one for the RHBD design, were used for the radiation transport simulations. The models themselves are quite large— $110 \mu\text{m} \times 85 \mu\text{m} \times 75 \mu\text{m}$ in the case of the baseline design and $217 \mu\text{m} \times 85 \mu\text{m} \times 75 \mu\text{m}$ for the RHBD design.

of each volume is determined by the normal-incident cross section of the broadbeam heavy ion data, which includes ^{22}Ne , ^{40}Ar , and ^{129}Xe . The weights and depths of each of the volumes are calculated by correlating microbeam data to TCAD simulations, both of which have been discussed previously [19]–[21]. This model was used in a fully reconstructed 3-D model of a shift register stage for all subsequent simulations, including the calibration steps described in Section III-A and the event rate calculations in Section IV. An image of this 3-D model is shown in Fig. 5. The response model shown in Fig. 4 is sufficient to model one stage of the shift register chain in [7]. More volume sets can be used for further variance reduction if necessary.

An important feature of the model shown in Fig. 4 is that it is scalable within the limits evaluated here. The transistors in the baseline and RHBD designs are different sizes. The RHBD transistors are $0.5 \times 2.5 \mu\text{m}^2$, whereas the baseline transistors

are $0.5 \times 1.0 \mu\text{m}^2$. The difference in transistor size accounts for some of the cross section difference between the baseline and RHBD designs for the argon and xenon data. The model dimensions can be adjusted within reason to account for the size difference without making drastic geometrical or phenomenological changes. The top-down areal cross section is dictated by the data and does not require modification.

The volume depth and weight need to be modified for different transistor sizes because the geometry of the subcollector junction changes with the emitter length. A larger junction presents a larger solid angle to mobile minority carriers in the substrate, which results in higher collection efficiency. A larger junction also results in deeper potential push-out, though this only occurs to a point, plateauing around $18\text{--}20 \mu\text{m}$ below the base-collector junction, which is located at the surface of the shallow trench isolation.

C. Response Model Implications

Recalling the ion strikes highlighted in Fig. 3, the linear combination of fiducial volumes shown in Fig. 4 approximates both ion strike conditions. It is clear that the most collected charge will result from normally incident strikes within the region bounded by the DTI. Since the broadbeam data in Fig. 2 show nearly constant cross sections over angle, with the exception of the RHBD data for neon and argon, the larger fiducial volumes have an aspect ratio close to unity.

It is important to note that using a model of weighted fiducial volumes in a linear combination, as is done here, is not a single-point solution. The combination of the fiducial volumes does not have to be linear; it can be non-linear continuous like a polynomial or even discontinuous if logic tests are added in order to add more advanced correlation. The model employed here is part of a much more generalized class of approximations that can be applied to many different situations. See the models in [13] and [14] where a linear combination of fiducial volumes is used to model heavy ion, proton, and neutron data in a $0.25 \mu\text{m}$ CMOS SRAM.

III. MODEL CALIBRATION

A. Heavy Ion Response

Before computing on-orbit event rates, the model was verified against data sets that covered enough of the possible response-parameter space to ensure predictable behavior in a more diverse environment such as geosynchronous or low-earth orbit. The model described in Section II-B was calibrated to the heavy ion datasets for the baseline and RHBD designs shown in Fig. 2.

In each of the two cases, the calibration scheme is the same and follows this general procedure.

- 1) Size top-down area of all three fiducial volumes corresponding to their counterpart heavy ion cross section at normal incidence—neon, argon, and xenon in this case.
 - a) This step excludes the volume contained entirely within the DTI, labeled with a weight of 0.8 in Fig. 4. The normally incident neon cross section is slightly larger than the in-trench silicon area in both the baseline and RHBD design data.

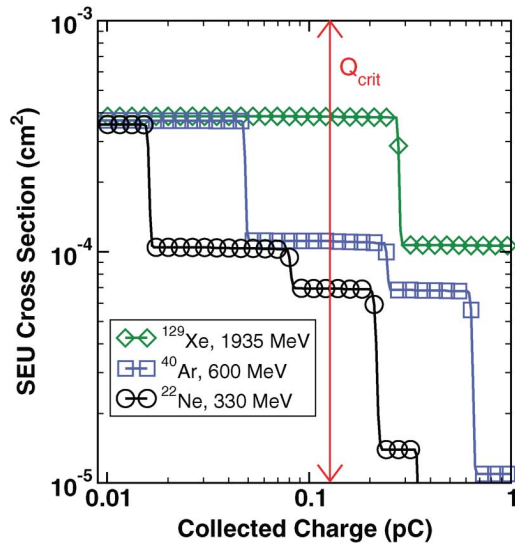


Fig. 6. This figure shows simulated charge collection cross sections at normal incidence for the baseline shift register design. The Q_{crit} is chosen so that the extracted cross section most closely matches the dataset in question. Data markers are sparse to aid viewing.

- 2) Infer the thickness and weight of each volume from microbeam or laser test data and TCAD simulations. The numbers listed in Fig. 4 are appropriate starting values.
- 3) Simulate all ions in the dataset at normal incidence to check that this simplest case returns the correct result.
 - a) At this point, a critical charge must be determined so that the cross section can be evaluated with consistency for all ion species and angles. An example cross section collected charge curve is shown in Fig. 6.
- 4) Simulate each set of ion angles individually and make minor adjustments to the thickness and weight of the appropriate fiducial volumes.
- 5) Finally, in order to gain a self-consistent solution, all data points must be simulated, the results evaluated using the same critical charge value, and an accurate match to all data achieved.

At this point, it is important to mention a feature of the simulation results displayed in Fig. 6: the device sensitivity is dominated by direct ionization from the primary incident particle. This fact could also be derived from the low SEU threshold in combination with the knowledge of large charge collection volumes. Regardless of this fact, all simulations were carried out with complete physics lists, including the Geant4 binary intra-nuclear collision cascade [34] to determine the final state for ion-ion nuclear reactions.

The calibrated heavy ion results for both the baseline and RHBD circuit designs are shown in Fig. 7(a) and (b). The Q_{crit} for each of the calibrations is displayed on the individual figures.

B. Proton Calibration Results

The experimental data shown in Fig. 2 were gathered and published in 2005 [7] and only included heavy ion cross sections. Proton data were collected during recent experiments on the CREST chip [7] at the Crocker Nuclear Laboratory (CNL) at the University of California at Davis using 63 MeV protons.

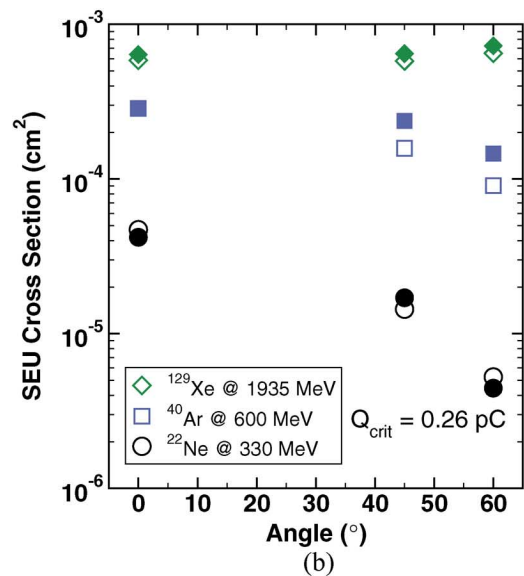
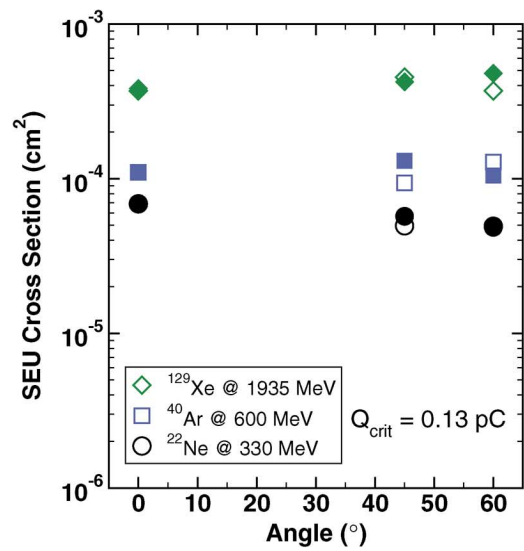


Fig. 7. Plots (a) and (b) show the calibrated results of the computer simulations for the entire 127-stage shift register from [7]. In each case the open symbols are the data from Fig. 2 and the closed symbols are the derived simulation results from output similar to that shown in Fig. 6. (a) Baseline design heavy ion calibration; (b) RHBD heavy ion calibration.

As with other high-speed bit error rate tests, all the cross sections reported refer to the event cross section and not the error (number of upset bits in an event) cross section. This also applies to the heavy ion data already presented.

These data were taken on the baseline and RHBD designs at several different data rates at normal incidence and a grazing angle. The full data set is plotted in Fig. 8(a). For reference, the baseline design is the nominal switching architecture from [7] and the RHBD design is the dual-interleaved architecture from [7]. The test was conducted using the CREST on-board data and clock generation, but the events were recorded using an external Anritsu MP1764C error detector, which is part of a bit error rate test (BERT) system. This data set is consistent with other SiGe HBT high-speed proton tests [5], [9]. The cross section is approximately constant across different data rates.

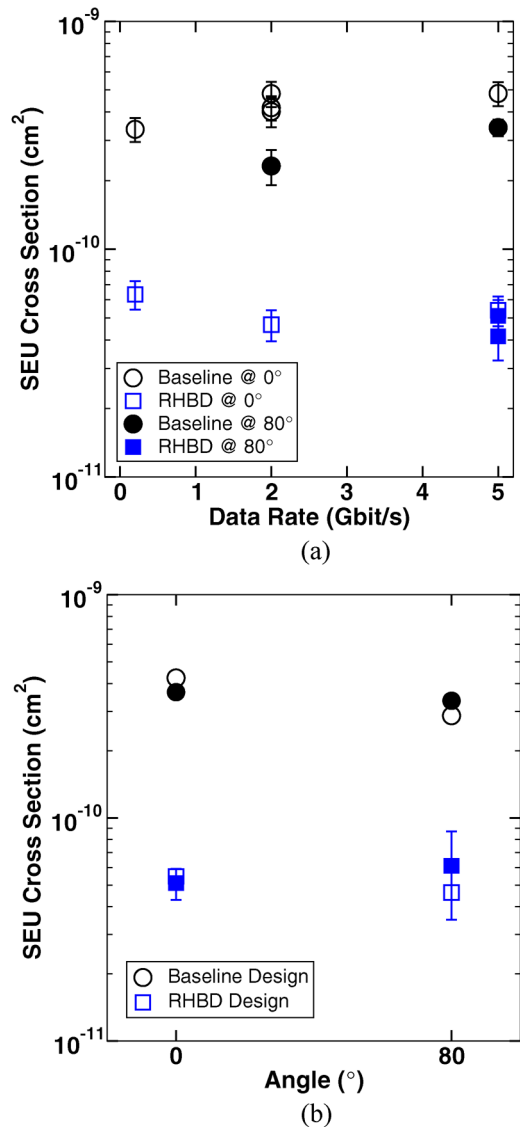


Fig. 8. (a) 63 MeV proton data from CNL taken on the baseline and RHBD CREST chip designs. In [7] these were referred to as the nominal switching current (baseline) and dual-interleaved (RHBD) architectures. The error bars are 1σ and represent the propagation of a 10% fluence error and a 1σ statistical error on the number of events recorded. (b) A comparison between the proton data from (a) and simulation results based on the model described in Section II-B, which was calibrated to heavy ion data. The strong agreement shown above was obtained by simply changing the particle and energy in the simulation; no further adjustments were made. The open symbols are data based on the average across data rate from (a) and the solid symbols are simulation results using the response model. Error bars, shown if they are bigger than the data marker, are 1σ statistical errors.

This data set can now be used to check the proton response of the model developed in the previous section. These modeling results are shown in Fig. 8(b). The data shown in Fig. 8(b) are the average cross section across data rate since the simulation model cannot take data rate into account, something that is the subject of current investigations.

As in previous modeling scenarios [14], the heavy ion model was validated against proton data by only a change of particle and energy in the simulation environment. The strong match between simulation and data validates a larger portion of the model's acceptable parameter space, making it usable for environments with large proton fluxes. These simulation results

were obtained from the model calibrated with heavy ion data only; no further adjustment was required.

IV. EVENT RATE CALCULATIONS

A. Geosynchronous and Low-Earth Orbit Event Rates

MRED, used for the modeling throughout this work, has the ability to import and sample across pre-defined particle flux spectra [11], [12]. CREME96 [35] was used to generate the particle flux spectra for the geosynchronous (GEO) and low-earth orbit (LEO) environments, but CREME96 was not used to perform the rate calculations. Both of the environments were solar minimum/quiet conditions, included available ion species from $1 \leq Z \leq 92$, and assumed 100 mil of aluminum shielding. The LEO spectra were for the space station orbit, which, according to CREME96, is at an inclination of 51.6° and an orbital radius of 500 km. The rate prediction methodology used to carry out the computations is described in [11] and [12].

The environment computations for the baseline and RHBD designs used the simulated energy deposition from approximately 5×10^8 individual events with a hadronic cross section bias factor of 75. The bias factor serves to reduce the variance for very rare events by increasing their occurrence in a statistically well-defined manner. In previous cases [11], the bias factor was set to 200. However, if the bias factor is set too high, too many primary particles are consumed in nuclear reactions, artificially depleting the transmitted flux on the backside of the target, which is non-physical. The target, shown in Fig. 5, is large and quite thick, about $110 \mu\text{m} \times 85 \mu\text{m} \times 75 \mu\text{m}$, so backside flux depletion is an issue. All ions simulated were incident on the target uniformly over 4π steradians for both GEO and LEO environments.

The event rates for both GEO and LEO environments are plotted in Fig. 9(a) and (b). The rates shown for each ion in the environmental spectrum have been reverse integrated, from right-to-left, so that the total event rate for each design, at a particular critical charge, is that rate or less.

There is a $1.6 \times$ to $6.2 \times$ difference between the total rate for the baseline and RHBD designs due to the higher critical charge of the RHBD design. The dominant contribution to each of the four rate curves shown comes from $25 \leq Z \leq 30$, which are the elements manganese, iron, cobalt, copper, and zinc. This large contribution is due to the fact that many of these impinging ions have high stopping powers in conjunction with significant flux. The contributions of these five ions approach the contributions from the other 81 ions that were simulated; this is true for both GCR and LEO event rates. However, in LEO orbits, the flux of these key ions is much lower due to natural magnetic shielding, leading to the lower event rate.

The baseline and RHBD curves shown in Fig. 9(a) and (b) appear in a counterintuitive way since the rate curve for the RHBD device is above the baseline device. However, the RHBD device has a larger subcollector junction area by a factor of approximately 1.6 since it is a bigger device relative to the baseline design. The rate curve of the RHBD design is higher since the area of the subcollector junction plays a significant role in the device's response to charge liberated from ionizing radiation.

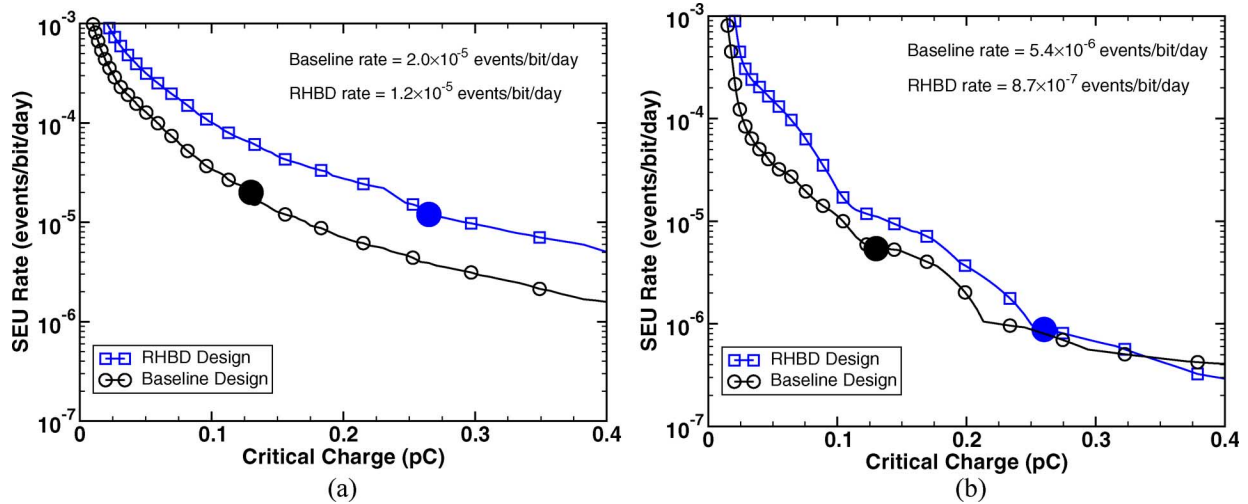


Fig. 9. These figures show the simulated event rates for the two shift register designs. The LEO event rate is approximately one order of magnitude below the GCR event rate due to sensitivity dominated by direct ionization and the reduced flux of many significant contributors. There is a $1.6\times$ to $6.2\times$ difference between the event rates for the baseline and RHBD designs. The data markers have been thinned to aid viewing. The large markers show where the rate was evaluated based on the critical charge derived from the fit shown in Fig. 7(a) and (b)—0.13 pC and 0.26 pC. (a) Geosynchronous orbit event rate; (b) low-earth orbit event rate.

The environment-based SEU rates presented are to be interpreted as event rates, not error rates. The energy deposition response model developed in Section II-B makes no attempt to derive temporal or event-composition information—i.e., zero-to-one, one-to-zero, flatten-to-one, flatten-to-zero, mangle, etc. [36]. The model neither calculates the number of upset bits in the event nor yields any information regarding preferences for burst error modes. However, the model makes the most accurate representation to date by providing an energy deposition response behavior consistent with device geometry and the charge collection mechanisms present in this type of process technology.

The present modeling approach is the first and necessary step towards solving the more intricate, time-dependent problem, which requires the energy deposition model to adapt its properties and volume-to-volume logic dynamically. Such a model would also have to be tied to a circuit-level simulator with compact models in order to produce burst error information reliably. In addition to those non-trivial steps, there is a great need for experimentally measured radiation-induced current transients in SiGe HBT BiCMOS process technology. Current commercial TCAD simulators have been successful at modeling the total collected charge from radiation events [19]–[21], [24], [37], but there are no experimental data with which to compare the induced current transients. It is believed that the present TCAD radiation-induced transients are inaccurate in some regimes. Experiments and simulations are currently underway to make these types of high-bandwidth transient measurements and continue advancing the state-of-the-art in energy deposition response modeling.

V. CONCLUSION

The shape and relationship between the fiducial volumes represents a critical aspect of this study. The fiducial volumes explain in a quantitative and qualitative way the once-anomalous angular response of the technology, the low SEU threshold, and the large saturated cross section observed for the most

highly ionizing particles. Putting this model together unifies many years of experimental and theoretical work and provides intuition to designers considering SiGe HBT projects. It also opens the door for more complex types of modeling that will begin to look at time-domain effects and other aspects of extreme, high-speed digital technologies like this.

ACKNOWLEDGMENT

The authors would like to thank K. LaBel, L. Cohn, the Special Purposes Processor Group at the Mayo Foundation, and D. M. Fleetwood. Thanks are also due to AJ KleinOowski, G. D. Carpenter, and IBM Research for supporting the author during manuscript preparation and the Nuclear and Space Radiation Effects Conference. This work was conducted in part using the resources of the Advanced Computing Center for Research and Education (ACCRES) at Vanderbilt University, Nashville, TN.

REFERENCES

- [1] J. D. Cressler, M. C. Hamilton, G. S. Mullinax, Y. Li, G. Niu, C. J. Marshall, P. W. Marshall, H. S. Kim, M. J. Palmer, A. J. Joseph, and G. Freeman, "The effects of proton irradiation on the lateral and vertical scaling of UHV/CVD SiGe HBT BiCMOS technology," *IEEE Trans. Nucl. Sci.*, vol. 47, no. 6, pp. 2515–2520, Dec. 2000.
- [2] A. K. Sutton, B. M. Haugerud, Y. Lu, W. M. L. Kuo, J. D. Cressler, P. W. Marshall, R. A. Reed, J. S. Rieh, G. Freeman, and D. Ahlgren, "Proton tolerance of fourth-generation 350 GHz UHV/CVD SiGe HBTs," *IEEE Trans. Nucl. Sci.*, vol. 51, no. 6, pp. 3736–3742, Dec. 2004.
- [3] J. D. Cressler, "On the potential of SiGe HBTs for extreme environment electronics," *Proc. IEEE*, vol. 93, pp. 1559–1582, Sep. 2005.
- [4] P. W. Marshall, M. A. Carts, A. Campbell, D. McMorro, S. Buchner, R. Stewart, B. Randall, B. Gilbert, and R. A. Reed, "Single-event effects in circuit-hardened SiGe HBT logic at gigabit per second data rates," *IEEE Trans. Nucl. Sci.*, vol. 47, no. 6, pp. 2669–2674, Dec. 2000.
- [5] R. A. Reed, P. W. Marshall, J. C. Pickel, M. A. Carts, B. Fodness, G. F. Niu, K. Fritz, G. Vizkelethy, P. E. Dood, T. Irwin, J. D. Cressler, R. Krishivasan, P. Riggs, J. Prairie, B. Randall, B. Gilbert, and K. A. LaBel, "Heavy-ion broad-beam and microprobe studies of single-event upsets in a 0.20 μm SiGe HBT heterojunction bipolar transistors and circuits," *IEEE Trans. Nucl. Sci.*, vol. 50, no. 6, pp. 2184–2190, Dec. 2003.

- [6] P. W. Marshall, M. Carts, A. Campbell, R. Ladbury, R. Reed, C. Marshall, S. Currie, D. McMorrow, S. Buchner, S. Seidleck, P. Riggs, K. Kritz, B. Randall, and B. Gilbert, "A comparative study of heavy-ion and proton-induced nit-error sensitivity and complex burst error modes in commercially available high-speed SiGe BiCMOS," *IEEE Trans. Nucl. Sci.*, vol. 51, no. 6, pp. 3457–3463, Dec. 2004.
- [7] P. W. Marshall, M. A. Carts, S. M. Currie, R. A. Reed, B. Randall, K. Fritz, K. Kennedy, M. Berg, R. Krithivasan, and C. Siedlick, "Autonomous bit error rate testing at multi-Gbit/s rates implemented in a 5AM SiGe circuit for radiation effects self test (CREST)," *IEEE Trans. Nucl. Sci.*, vol. 52, no. 6, pp. 2446–2454, Dec. 2005.
- [8] R. Krithivasan, Y. Lu, J. D. Cressler, J.-S. Rieh, M. H. Kater, D. Ahlgren, and G. Freeman, "Half-terahertz operation of SiGe HBTs," *IEEE Electron. Device Lett.*, vol. 27, pp. 567–569, Jul. 2006.
- [9] D. L. Hansen, P. Chu, K. Jobe, A. L. McKay, and H. P. Warren, "SEU cross sections of hardened and unhardened SiGe circuits," *IEEE Trans. Nucl. Sci.*, vol. 53, no. 6, pp. 3579–3586, Dec. 2006.
- [10] K. M. Warren, R. A. Weller, M. H. Mendenhall, R. A. Reed, D. R. Ball, C. L. Howe, B. D. Olson, M. L. Alles, L. W. Massengill, R. D. Schrimpf, N. F. Haddad, S. E. Doyle, D. McMorrow, J. S. Melinger, and W. T. Lotshaw, "The contribution of nuclear reactions to heavy ion single event upset cross section measurements in a high-density SEU hardened SRAM," *IEEE Trans. Nucl. Sci.*, vol. 52, no. 6, pp. 2125–2131, Dec. 2005.
- [11] R. A. Reed, R. A. Weller, R. D. Schrimpf, M. H. Mendenhall, K. M. Warren, and L. W. Massengill, "Implications of nuclear reactions for single event effects test methods and analysis," *IEEE Trans. Nucl. Sci.*, vol. 53, no. 6, pp. 3356–3362, Dec. 2006.
- [12] R. A. Reed, R. A. Weller, M. H. Mendenhall, J.-M. Lauenstein, K. M. Warren, J. A. Pellish, R. D. Schrimpf, B. D. Sierawski, L. W. Massengill, P. Dodd, N. F. Haddad, R. K. Lawrence, J. H. Bowman, and R. Conde, "Impact of ion energy and species on single event effects analysis," *IEEE Trans. Nucl. Sci.*, vol. 54, no. 6, Dec. 2007.
- [13] K. M. Warren, B. D. Sierawski, R. A. Weller, R. A. Reed, M. H. Mendenhall, J. A. Pellish, and R. D. Schrimpf, "Predicting thermal neutron induced soft errors in static memories using TCAD and physics-based Monte Carlo simulation tools," *IEEE Electron Device Lett.*, vol. 28, pp. 180–182, Feb. 2007.
- [14] K. M. Warren, R. A. Weller, B. D. Sierawski, R. A. Reed, M. H. Mendenhall, R. D. Schrimpf, L. W. Massengill, M. Porter, J. Wilkinson, K. A. LaBel, and J. H. Adams, Jr., "Application of RADSAFE to model single event upset response of 0.25 μm CMOS SRAM," *IEEE Trans. Nucl. Sci.*, vol. 54, no. 4, pp. 898–903, Aug. 2007.
- [15] C. L. Howe, R. A. Weller, R. A. Reed, M. H. Mendenhall, R. D. Schrimpf, K. M. Warren, D. R. Ball, L. W. Massengill, K. A. LaBel, J. W. Howard, and N. F. Haddad, "Role of heavy-ion nuclear reactions in determining on-orbit single event error rates," *IEEE Trans. Nucl. Sci.*, vol. 52, no. 6, pp. 2182–2188, Dec. 2005.
- [16] A. S. Koybayashi, D. R. Ball, K. M. Warren, R. A. Reed, N. Haddad, M. H. Mendenhall, R. D. Schrimpf, and R. A. Weller, "The effect of metallizations layers on single event susceptibility," *IEEE Trans. Nucl. Sci.*, vol. 52, no. 6, pp. 2189–2193, Dec. 2005.
- [17] D. C. Ahlgren, G. Freeman, S. Subbanna, R. Groves, J. Greenberg, J. Malinowski, D. Nguyen-Ngoc, S. J. Jeng, K. Stein, K. Schonenberg, D. Kiesling, B. Martin, S. Wu, D. L. Harame, and B. S. Meyerson, "A SiGe HBT BiCMOS technology for mixed-signal RF applications," in *Proc. IEEE Bipolar/BiCMOS Circuits and Tech. Meeting*, Minneapolis, MN, 1997, pp. 195–198.
- [18] R. Krithivasan, G. F. Niu, J. D. Cressler, S. M. Currie, K. E. Fritz, R. A. Reed, P. W. Marshall, P. A. Riggs, B. A. Randall, and B. Gilbert, "An SEU hardening approach for high-speed SiGe HBT digital logic," *IEEE Trans. Nucl. Sci.*, vol. 50, no. 6, pp. 2126–2134, Dec. 2003.
- [19] E. J. Montes, R. A. Reed, J. A. Pellish, M. L. Alles, R. D. Schrimpf, R. A. Weller, M. Varadharajaperumal, G. Niu, A. K. Sutton, R. Diestelhorst, G. Espinel, R. Krithivasan, J. P. Comeau, J. D. Cressler, P. W. Marshall, and G. Vizkelethy, "Single event upset mechanisms for low energy deposition events in silicon germanium HBTs," presented at the IEEE Nuclear Space Radiation Effects Conf., Ponte Vedra Beach, FL, Jul. 2006.
- [20] J. A. Pellish, R. A. Reed, R. D. Schrimpf, M. L. Alles, M. Varadharajaperumal, G. Niu, A. K. Sutton, R. Diestelhorst, G. Espinel, R. Krithivasan, J. P. Comeau, J. D. Cressler, G. Vizkelethy, P. W. Marshall, R. A. Weller, M. H. Mendenhall, and E. J. Montes, "Substrate engineering concepts to mitigate charge collection in deep trench isolation technologies," *IEEE Trans. Nucl. Sci.*, vol. 53, no. 6, pp. 3298–3305, Dec. 2006.
- [21] M. Varadharajaperumal, G. F. Niu, R. Krithivasan, J. D. Cressler, R. A. Reed, P. W. Marshall, G. Vizkelethy, P. E. Dodd, and A. J. Joseph, "3-D simulation of heavy-ion induced charge collection in SiGe HBTs," *IEEE Trans. Nucl. Sci.*, vol. 50, no. 6, pp. 2191–2198, Dec. 2003.
- [22] P. Chu, D. L. Hansen, B. L. Doyle, K. Jobe, R. Lopez-Aguado, M. Shoga, and D. S. Walsh, "Ion-microbeam probe of high-speed shift registers for SEE analysis—Part I: SiGe," *IEEE Trans. Nucl. Sci.*, vol. 53, no. 3, pp. 1574–1582, Jun. 2006.
- [23] R. A. Reed, G. Vizkelethy, J. A. Pellish, B. D. Sierawski, K. M. Warren, M. Porter, J. Wilkinson, P. W. Marshall, G. Niu, J. D. Cressler, R. D. Schrimpf, A. D. Tipton, and R. A. Weller, "Applications of heavy ion microprobe for single-event effects analysis," *Nucl. Instrum. Methods B*, vol. 261, pp. 443–446, Jul. 2007.
- [24] A. K. Sutton, M. Bellini, J. D. Cressler, J. A. Pellish, R. A. Reed, P. W. Marshall, G. Niu, G. Vizkelethy, M. Turowski, and A. Raman, "An evaluation of transistor-layout RHBD techniques for SEE mitigation in SiGe HBTs," *IEEE Trans. Nucl. Sci.*, vol. 54, no. 6, Dec. 2007.
- [25] G. Vizkelethy, R. A. Reed, P. W. Marshall, and J. A. Pellish, "Ion beam induced charge (IBIC) studies of silicon germanium heterojunction bipolar transistors (HBTs)," *Nucl. Instrum. Methods B*, vol. 260, pp. 264–269, Jul. 2007.
- [26] E. L. Petersen, J. C. Pickel, J. H. Adams, Jr., and E. C. Smith, "Rate predictions for single-event effects—A critique," *IEEE Trans. Nucl. Sci.*, vol. 39, no. 6, pp. 1577–1599, Dec. 1992.
- [27] E. L. Petersen, J. C. Pickel, E. C. Smith, P. J. Rudeck, and J. R. Letaw, "Geometrical factors in SEE rate calculations," *IEEE Trans. Nucl. Sci.*, vol. 40, no. 6, pp. 1888–1909, Dec. 1993.
- [28] L. W. Connell, F. W. Sexton, and A. K. Prinza, "Further development of the heavy ion cross section for single event UPset model: (HICUP)," *IEEE Trans. Nucl. Sci.*, vol. 42, no. 6, pp. 2026–2034, Dec. 1995.
- [29] F. W. Sexton, J. S. Fu, R. A. Kohler, and R. Koga, "SEU characterization of a hardened CMOS 64 K and 256 K SRAM," *IEEE Trans. Nucl. Sci.*, vol. 36, no. 6, pp. 2311–2317, Dec. 1989.
- [30] C.-M. Hsieh, P. C. Murley, and R. R. O'Brien, "A field-funneling effect on the collection of alpha-particle-generated carriers in silicon devices," *IEEE Electron Device Lett.*, vol. 2, pp. 103–105, Apr. 1981.
- [31] C.-M. Hsieh, P. C. Murley, and R. R. O'Brien, "Dynamics of charge collection from alpha-particle tracks in integrated circuits," in *Proc. Int. Reliability Physics Symp.*, Orlando, FL, Apr. 1981, pp. 38–42, IEEE.
- [32] C.-M. Hsieh, P. C. Murley, and R. R. O'Brien, "Collection of charge from alpha-particle tracks in silicon devices," *IEEE Trans. Electron Devices*, vol. 30, pp. 686–693, Jun. 1983.
- [33] C. Hu, "Alpha-particle-induced field enhanced collection of carriers," *IEEE Electron Device Lett.*, vol. 3, pp. 31–34, Feb. 1982.
- [34] G. Folger, V. N. Ivanchenko, and J. P. Wellisch, "The binary cascade: Nucleon nuclear reactions," *Eur. Phys. J. A*, vol. 21, pp. 407–417, Sep. 2004.
- [35] A. J. Tylka, J. H. Adams, Jr., P. R. Boberg, B. Brownstein, W. F. Dietrich, E. O. Flueckiger, E. L. Petersen, M. A. Shea, D. F. Smart, and E. C. Smith, "CREME96: A revision of the cosmic ray effects on micro-electronics code," *IEEE Trans. Nucl. Sci.*, vol. 44, no. 6, pp. 2150–2160, Dec. 1997.
- [36] A. K. Sutton, R. Krithivasan, P. W. Marshall, M. A. Carts, C. Siedleck, R. Ladbury, J. D. Cressler, C. J. Marshall, S. Currie, R. A. Reed, G. Niu, B. Randall, K. Fritz, D. McMorrow, and B. Gilbert, "SEU error signature analysis of Gbit/s SiGe logic circuits using a pulsed laser microprobe," *IEEE Trans. Nucl. Sci.*, vol. 53, no. 6, pp. 3277–3284, Dec. 2006.
- [37] J. P. Comeau, R. Krithivasan, A. K. Sutton, R. Diestelhorst, G. Espinel, A. P. Gnana Prakash, B. Jun, J. D. Cressler, M. Varadharajaperumal, G. Niu, J. A. Pellish, R. A. Reed, P. W. Marshall, and G. Vizkelethy, "An investigation of transistor layout-based SEU hardening of SiGe HBTs," presented at the IEEE 8th Eur. Conf. Radiation Its Effects on Components and Systems, Athens, Greece, Sep. 2006, Paper A-2.